CHAPTER 4

Anomalous Hall effect in Cu doped Bi_2Te_3 Topological Insulator

4.1 Introduction:

Topological insulators (TIs) with insulating bulk but conducting surface state with characteristic Dirac dispersion and mass- less Dirac fermions, have attracted much attention due to many exotic properties[81]. The spins of the electrons at the surface are locked in the perpendicular direction of momentum due to the strong spin–orbit interaction which is protected by time- reversal symmetry (TRS). These polarized spins at the surfaces may find application in quantum computation and spintronic devices. Moreover, quantum oscillations i.e. Shubnikov–de- Haas (SdH) oscillations in transport experiments can be seen only at low temperatures and at high magnetic fields in very good quality crystals [19] which is one of the much effective tools to investigate the topology of the Fermi surface. The measurement accuracy in the determination of Fermi surface cross- sectional areas is better than 0.1% of the area of the Brillouin zone whereas in case of effective masses accuracy is better than 5% [82]. Bi_2Te_3 is one of the most attractive element among A_2B_3 series (A = Bi, Sb and B = Te, Se), having n-type of carrier density due to a large amount of Te vacancies [81], [83]. Tuning of carrier type has been observed with doping very high concentration (x = 0.30) of magnetic element Fe in Bi_2Te_3 [84] which may destroy the TRS. 3D transition metal doped TIs have been studied since a decade in which Cu doped Bi based TIs have many intriguing properties such as Superconductivity, structural defects etc. [85], [86]. Properties of nano-plates and nanoflower of Cu doped Bi_2Te_3 have been thoroughly studied [87]–[89]. However, in most of the reports Cu has been doped on Bi site [90].But this will also induce charge carriers in the compound due to the difference in natural valency (divalent Cu and trivalent Bi). On the other hand, both Te and Cu is in diva- lent state and as a matter of fact the replacement of Te by Cu will not generate any additional charge carrier. Defect induced room temperature

ferromagnetism (RTFM) has been shown in our previous report [60] at the doping concentration x = 0.15 in the Cu doped Bi_2Te_3 TI. Moreover, finding anomalous Hall effect [6] in topological states of matter is highly interesting. In antiferromagnetic GdPtBi [91], whose electronic structure is similar to the topologically insulating HgTe, the existence of anomalous Hall effect has been reported. Normal Hall effect can be easily explained by Lorentz force but the mechanism of AHE is still controversial despite the long history of research. Generally, extrinsic scattering mechanism and intrinsic mechanism are responsible for the presence of AHE [44], [92]–[95]. Extrinsic scattering mechanism is similar to those which determine the transport coefficient whereas the intrinsic mechanism is independent of scattering. In the present work, we have investigated magnetic and magneto-transport properties of Cu doped Bi_2Te_3 samples. It has been observed that even in the non- magnetic state the AHE exists. Moreover, the information about the location of the Fermi energy in E–k diagram has been estimated from ARPES study which is in good agreement with the Hall data.

4.2 Experimental details

The single crystal $Bi_2Cu_xTe_{3-x}$ (x = 0.03, 0.09 and 0.15) were grown by two step melting method as has been reported elsewhere [60]. Obtained silver colored single crystals were easily cleaved along (00l) plane. Prepared single crystals were characterized by x-ray diffraction at room temperature. Magnetic measurements were carried out by using Quantum Design SQUID magnetic properties measurement system (MPMS). The electrical transport properties and magneto-transport measurements were performed by physical properties measurement system (PPMS). A rectangular shaped crystal of the order of 3mm × 1mm × 0.2mm was used for magneto-transport measurement and magnetic measurement and

measurement were performed by standard five probe method. Topological surface state of prepared samples was confirmed by laser-based angle-resolved photoemission spectroscopy (ARPES) at 20 K [61] at HiSOR, Hiroshima University, Japan under proposal no. 17AG052.

4.3 Results and discussions

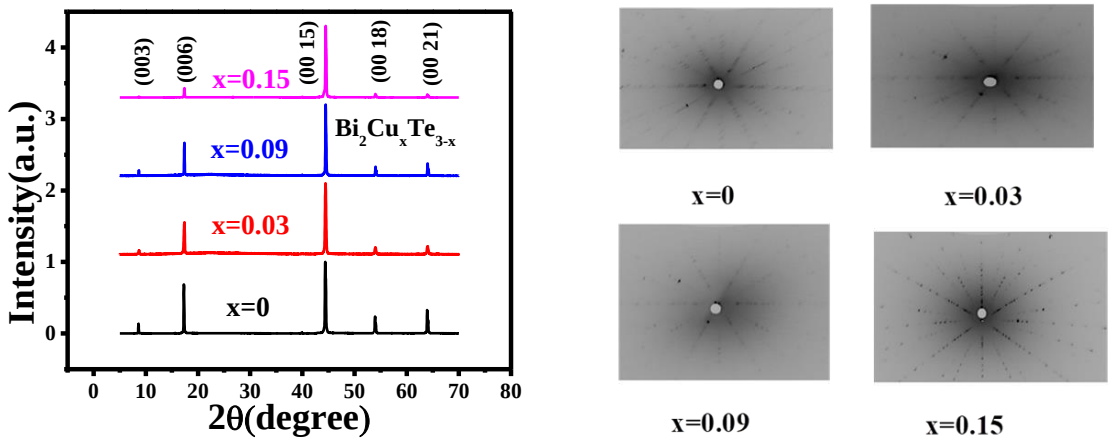

Figure 4.1: X-ray diffraction pattern of $Bi_2Cu_xTe_{3-x}$ topological insulators and Laue diffraction Pattern.

Table 4.1: Lattice parameters of $Bi_2Cu_xTe_3$ x (with x = 0, 0.03, 0.09 and 0.15) obtained from the Rietveld refinement.

Composition	a(Å)	b(Å)	c(Å)
X=0	4.381	4.381	30.462
X=0.03	4.382	4.382	30.466
X=0.09	4.383	4.383	30.470
X=0.15	4.380	4.380	30.464

Single crystals of $Bi_2Cu_xTe_{3-x}$ (x = 0, 0.03, 0.09, 0.15) with the cleaved surface along the basal planes (00l) were characterized using x-ray diffraction (XRD) as is shown in figure 4.1. XRD patterns clearly indicate the absence of any impurity. For further confirmation of the single crystallinity of the samples we have performed Laue experiment for x = 0, 0.03, 0.09 and 0.15 samples. The Laue pattern shows the excellent single crystalline nature of the as prepared samples (stacks.iop.org/JPhysCM/32/305602/mmedia). Around $2\theta = 54^\circ$ and 64° (figure 4.1), a small splitting due to the difference in the wavelength of x-ray source of CuK_α and CuK_β radiation is observed. An additional peak around $2\theta = 40^\circ$ for both the samples is observed which might be due to the slight misalignment or slight tilt angle of the crystallinity of as cleaved single crystals. The full width half maxima (FWHM) of the (003) peaks for the pure sample was very small (0.0960° 0.0014°) indicating that as prepared sample has excellent single crystallinity in long range. As we increase Cu concentration, the FWHM value increases implying that the crystallite size is decreasing with Cu content. If Cu is doped in a system, the lattice parameter 'c' can be increased or decreased depending on the position of Cu in the system[96], [97]. However, in our system the lattice parameters 'a' and 'c' almost remain constant. The observed slight variation can be explained by the occupancy of Cu entering either in the quintuple layers (substituting Bi or Te) or van der Waals gaps. Other possibility of this variation may be the low concentration of Cu which may lead inhomogeneity in the system[90], [98]. However, the obtained lattice parameter (given in table 4.1) is consistent with that of the reported value [99].

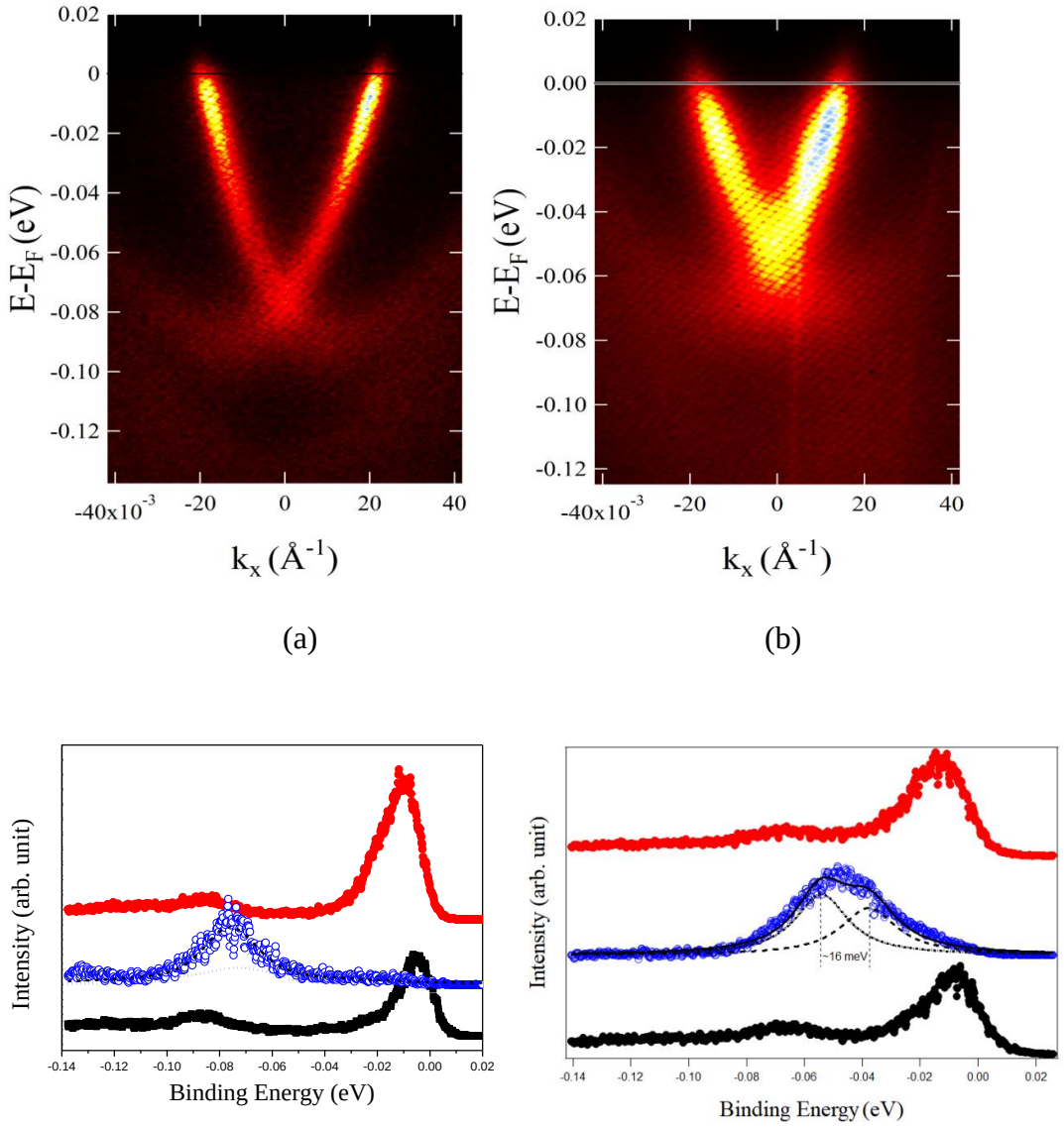

Figure 4.2: ARPES spectra for x = 0.03 (a) and 0.15 (b) of $Bi_2Cu_xTe_{3-x}$. (c) and (d) Show the electron distribution curve.

Energy dispersion curves acquired from laser ARPES for the samples x = 0.03 and 0.15 are shown in figure 4.2 (a) and 4.2 (b). The most prominently observed linearly dispersing electronic energy bands for both the samples are the surface-state bands (SSB) and are parts of the Dirac cones (DC). The DC lies in the binding energy range of 0 to 76 (±0.5) for x =0.03

and 0 to 57 (±0.5) meV for x = 0.15 samples. The DC consists of upper DC and lower DC touching each other at the Dirac point (DP) where one observes the spin degeneracy of the Dirac bands. The bulk valence band (BVB) can be easily seen below the DCs for the samples x = 0.03 and x = 0.15. Broadening of the bands within the DC for x = 0.15 sample is also observed in figure 4.2 (a) and 4.2 (b). This broadening might be attributed to the scattering centers produced by Cu, as scattering centers increase with the increase of Cu concentration in the host Bi_2Te_3. For better representation of the band structure, stacked intensity plots for the ARPES data are shown for the samples x = 0.03 and 0.15 in figure 4.3 (c) and 4.3 (d) respectively. To determine the band gap for surface carriers, present in the samples, we have tried a Lorentzian fitting of the energy distribution curve at the Γ point. For the x = 0.03 sample we have estimated a gap of less than 5 meV and for x = 0.15, the gap of less than 16 meV. Figure 4.2 (c) and 4.2 (d) show the energy distribution curves (EDCs) measured directly at the DP (at $k\| = 0$) (blue curves) and for opposite momenta relative to the Γ-point (red and black curves). Therefore, it is clear that on increasing doping concentration, band-gap is also increasing. Moreover, it is also clear from the ARPES plots that the DC for x = 0.15 is shifted toward lower binding energy in comparison to that for x = 0.03, indicating a p-type nature of Cu doped sample which is also consistent with the Hall and thermoelectric behavior of the samples[60].

Figure 4.3 (a) and 4.3 (b) show constant energy contours at the Fermi energy for x = 0.03 and 0.15 respectively. Circular con- tours in figure 4.3 (a) and 4.3 (b) depict Fermi surface (FS) due to the DC in the samples x = 0.03 and 0.15. Six petals around the FS arise from the FS sheets of the bulk valence band (BVB) which indicates that the Fermi energy apart from the DC is also crossing the BVB. The appearance of petals is not so much clear in x = 0.15

sample unlike x = 0.03 sample which might be due to the presence of large Cu concentration in x = 0.15 sample as the presence of Cu induces defects, distortion and scattering centers[1], [83], [100], [101].

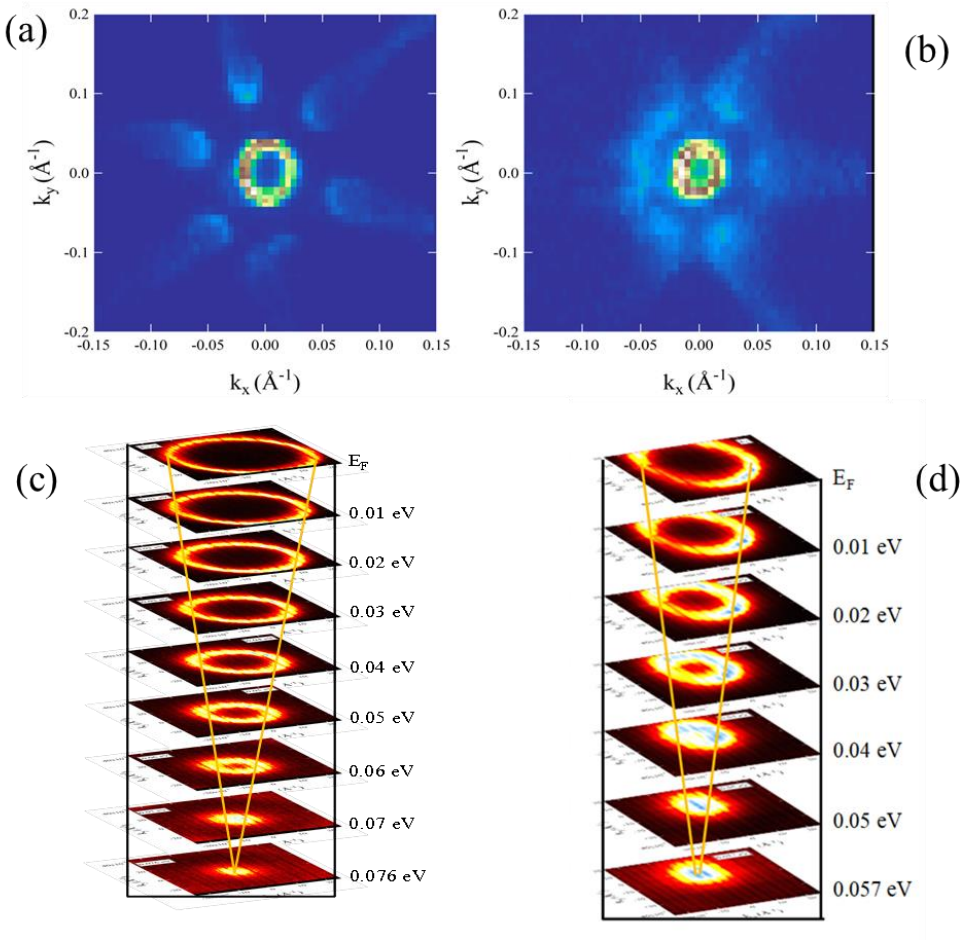

Figure 4.3: Constant energy contours of Bi2CuxTe3 x at the Fermi energy for (a) x = 0.03 and (b) 0.15 from ARPES measurement. (c) and (d) Show the stacked plots of the constant energy contours at different binding energies.

Figures 4.3 (c) and 4.3 (d) show the stacked plots of the constant energy contours at different binding energies from 0 meV (Fermi energy) to 76 meV (DP) for x = 0.03 and 57 meV (DP) for 0.15 samples respectively. It is clear from the graph that the shape of constant energy contour is circular for both the samples. Moreover, it is also clear from the graphs that

the area enclosed by the constant energy contour is decreasing as we go from the Fermi energy toward the DP, but the shape of the constant energy curve continues to remain circular for both the samples throughout. The absence of the hexagonal warping observed at the FS of the parent compound Bi2Te3 is due to the combined effect of the p-type doping as well as the reduction in the strength of spin–orbit coupling as we substitute Te by Cu[1]. The broadening of the constant energy contours as seen in the x = 0.15 sample as compared to that in the x = 0.03 sample might also be due to the increased scattering centers due to increased Cu content. The variation of longitudinal resistivity (ρ_{xx}) as a function of temperature under different magnetic fields for the samples x = 0.03 and 0.09 are shown in figure 4.4 whereas insets of figure 4.4 represent the resistivity behavior at different fields for x = 0 and x = 0.15 samples. We have also calculated residual resistivity ratio, defined as RRR = ρ_{xx} (300 K)/ρ_{xx} (2 K), where ρ_{xx} (300 K) and ρ_{xx} (2 K) is the resistivity at 300 K and 2 K respectively. The value of RRR for the sample x = 0 was 38 which was higher than the value reported by Shrestha et al[102]. Such large value of RRR indicates the high quality of crystals. However, as the Cu concentration increases RRR value decreases indicating the deterioration of crystal quality. The resistivity behavior of x = 0 and 0.03 suggest the presence of surface metallic conduction. A drastic change has been seen in the nature of resistivity curve for the higher Cu doped x = 0.09 and x = 0.15 samples. The presence of anomalies could be seen at different temperatures in both the samples. The anomalies become more significant at higher fields which are shown in figure 4.4 (b) and its inset. In x = 0.09 sample anomalies are located at 35 K, 90 K and 140 K [figure 4.4 (b)]. The scenario is little different in highest Cu doped sample where, the anomalies are shifted toward higher temperature in x = 0.15 sample and found at 50 K, 100 K, 150 K, 185 K and 285 K [inset of figure 4.4 (b)].

At higher temperature above 285 K, x = 0.15 sample is showing negative temperature coefficient unlike x = 0.09 sample, which is consistent with the reported results[19], [101], [103]–[105]. The upturn similar to the x = 0.09 and 0.15 has also been seen in some other reports[101], [104], the origin of which is not yet clear.

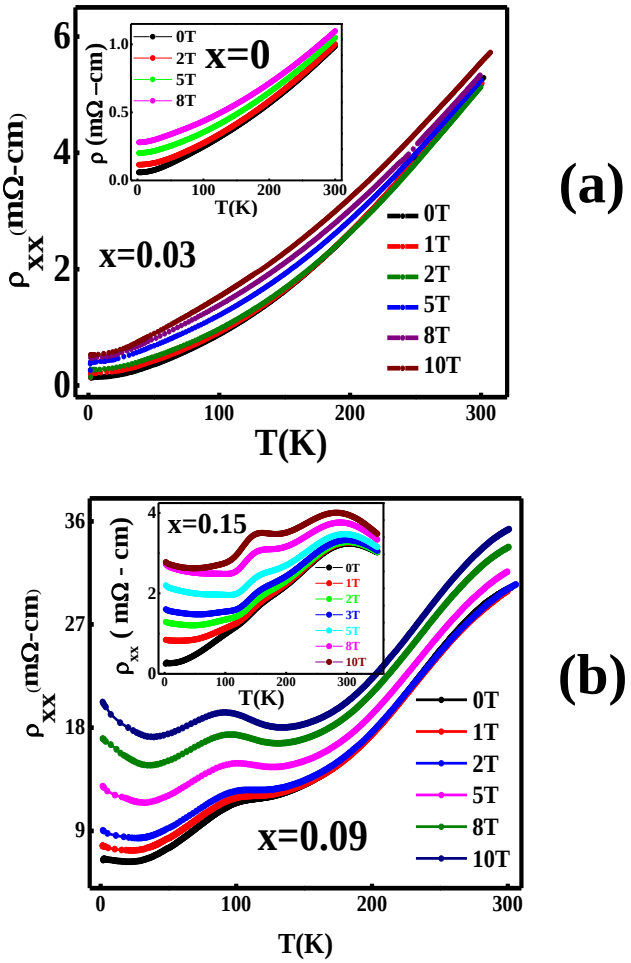

Figure 4.4: Temperature variation of resistivity of Bi2CuxTe3 x for (a) x = 0.03 and (b) 0.09.

The topological surface state has been already studied by several groups in pure Bi_2Te_3 using quantum oscillation in magneto-resistance measurement[102], [106]–[108]. Variation of magnetoresistance (MR) as a function of the applied magnetic field under different temperatures are shown in figure 4.5 for x = 0.03 and 0.09. Inset of figure 4.5 (b)

shows the MR behavior of x = 0.15 sample. Magnetoresistance (MR) of the samples is defined as, MR% = [R (H)−R (0)]/100 where R (H) is the resistance at applied magnetic field H, R (0) is the measured resistance at H = 0. It is obvious from the MR graph that it is completely symmetric for all the samples with respect to the reversal of the magnetic field direction, ruling out any possible contribution from Hall voltage. MR for all the samples increases with an applied magnetic field but decreases with increasing temperature. Increasing carrier concentration with temperature could be a reason for the decreasing MR value. Moreover, we have observed maximum MR value 1000% for x = 0.15 sample. Furthermore, MR curve shows a dip at low temperature indicating the existence of weak anti-localization (WAL)[109] as is observed in other TIs, the origin of which is π berry phase[110]. It is also observed from the MR curve that as the temperature is increased, MR dip broadened at the low field because at higher T, phase coherence length decreases [83]. Magnetic field in both the Cu doped samples x = 0.03 and 0.09 [shown in figure 4.5]. However, the oscillations are more prominent for the case of x = 0.09. Such type of oscillations in the magnetoresistance in metals are known as Shubnikov de-Hass (SdH) oscillations which has been also studied by various groups[111], [112]. For x = 0.15 no oscillation is observed even at the lowest possible temperature of measurement 2 K indicating that surface effect is increasing up to a certain concentration (x = 0.09) of Cu but it is reduced with further increase of Cu content.

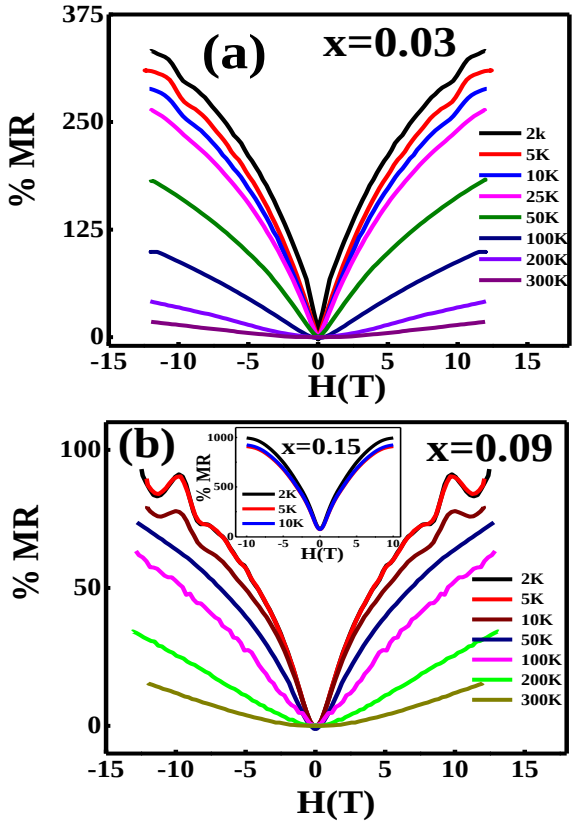

Figure 4.5: Magnetic field variation of magnetoresistance of $Bi_2Cu_xTe_{3-x}$ for (a) x = 0.03 and (b) 0.09 at different temperatures.

In order to further observe the clear quantum oscillations (observed in x = 0.09 and 0.03), $d\Delta R_{xx}$ at different temperatures have been plotted as a function of inverse magnetic field B^{-1} as shown in figures 4.6 (a) and 4.7 (a) [ΔR_{xx} has been determined by subtracting the smooth polynomial background from R_{xx}]. It is seen that amplitude of the oscillations decreases with the increase of temperature but frequency does not change for both the samples (figures 4.6 and 4.7). Presence of TSSs can be further confirmed by the value of Berry phase β which can be obtained by the Landau level fan diagram (figures 4.6 (b) and 4.7 (b)). The extracted value of β is 0.51 and 0.59 for x = 0.03 and 0.09 respectively, which is very close to 1/2 indicating that the oscillations originate from the surface helical state.

However, oscillation can depend on some other factors also. It deserves further study to throw light on the origin of observed oscillation.

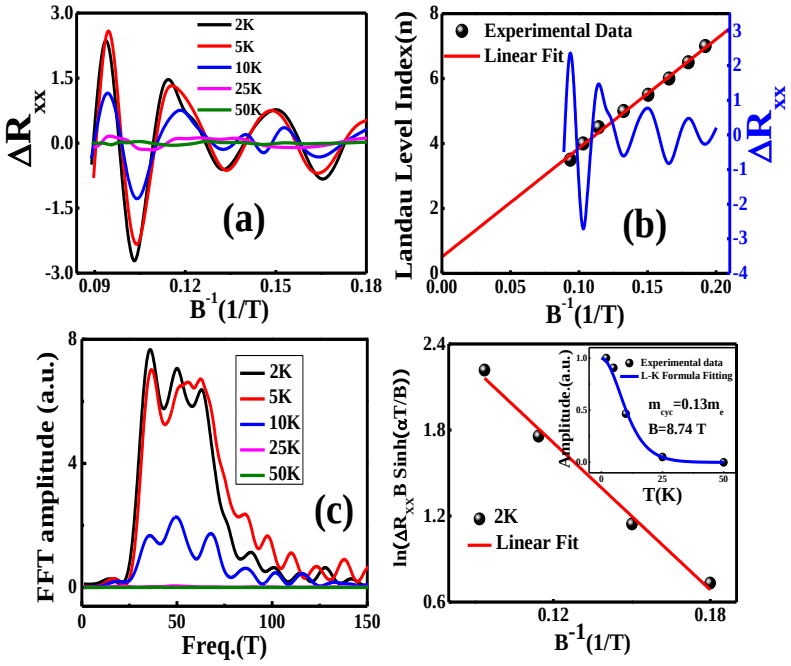

Figure 4.6: (a) SdH oscillations (b) Landau level fan diagram (c) first Fourier transform curve (d) L–K fitting curve and average calculated cyclotron mass (mcyc) [in inset of (d)] of Bi2CuxTe3−x for x =0.03.

Taking the circular assumption, $A = \pi k_f^2$ (A and k_f respectively being the Fermi cross section and Fermi momentum) we have determined the different parameters which have been shown in table 2. In order to identify the origin of the oscillations, we have also performed fast Fourier transforms (FFTs) at different temperatures corresponding to figures 4.6 (a) and 4.7 (a) [shown in figures 4.6 (c) and 4.7 (c)] for the sample x = 0.03 and x = 0.09. In order to determine the carrier concentration (n or p) and mobility (μ) of the undoped and doped samples, we have also carried out the Hall measurement at different temperatures. Figure 8 shows the variation of Hall resistivity as a function of applied magnetic field for the samples x = 0, 0.03, 0.09 and 0.15 at different temperatures and we have anti-symmetrized the Hall data before analysis. With Cu (x = 0.03, 0.09 and 0.15) doping slope changes from negative

(x = 0) to positive showing that carriers are tuned from n-type to p-type in the doped samples for the entire range of temperature of measurement which is also consistent with the ARPES results. Generation of electrons by TeBi anti site defects in the pure sample might be a reason for the tuning of charge carriers[19]. Variation of bulk carrier concentration as a function of temperature is shown in inset of figure 4.8 for all the samples. The estimated carrier concentration is well matched with the reported values in TIs[30], [84], [113], [114].

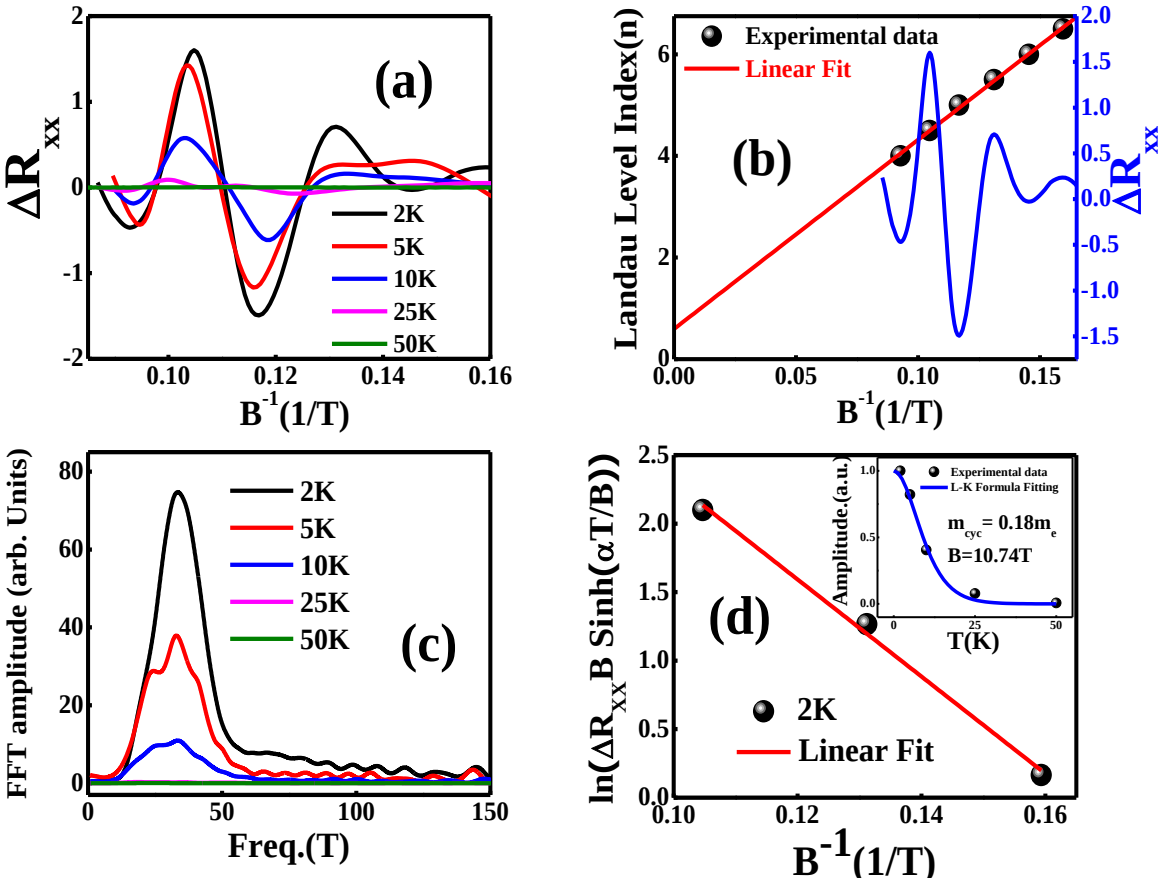

Figure 4.7: (a) SdH oscillations (b) Landau level fan diagram (c) first Fourier transform curve (d) L–K fitting curve and cyclotron mass calculation [in inset of (d)] of $Bi_2Cu_xTe_{3-x}$ for x = 0.09.

It is clear from n vs. T graph that carrier density increases with the increase in temperature. In fact, the topological surface state is a complete quantum phenomenon, and as a matter of fact, the surface effect will be significant at very low temperature. In consequence,

at very low-temperature surface state dominates over the bulk state and that is why the carrier concentration is low at low temperature ($T \leq 20$ K) and very large at high temperature.

Table 4.2: Obtained parameters of $Bi_2Cu_xTe_{3-x}$ (with x = 0.03 and 0.09) from SdH oscillations, first Fourier transform calculation and Hall effect measurements.

Obtained Parameter	**x=0.03**			**x=0.09**		
	SdH Oscillation Calculation	**FFT calculation**	**Hall calculation**	**SdH Oscillation Calculation**	**FFT calculation**	**Hall calculation**
Fermi momentum (K_f)	3.19×10^{8} m^{-1}	3.32×10^{8} m^{-1}	-	3.36×10^{8} m^{-1}	3.18×10^{8} m^{-1}	-
Surface carrier concentration (n_s)	1.62 $\times10^{12}/cm^2$	1.76 $\times10^{12}/cm^2$	-	1.80×10^{12} $/cm^2$	1.61×10^{12} $/cm^2$	-
Bulk carrier concentration (n_b)	1.09 $\times10^{18}/cm^3$	1.23 $\times10^{18}/cm^3$	8.635×10^{18}/ cm^3	1.28×10^{18}/ cm^3	$1.08\times10^{18}/cm^3$	$7.67\times10^{18}/cm^3$
Fermi velocity(v_f)	-	$2.94\times10^{5}ms^{-1}$	-	-	2.03×10^{5} ms^{-1}	-
Dingle Temperature(T_D)	-	9K	-	-	13K	-
Surface carrier life time(τ)	-	1.36× $10^{-13}s$	-	-	9.12× $10^{-14}s$	-

Mean Free Path(l)	-	40nm	-	-	19nm	-
mobility(μ)	-	239cm^2/Vs (Quantum mobility)	4.385×10^4cm^2/Vs (Hall mobility)	-	160cm^2/Vs (Quantum mobility)	1.9×10^3cm^2/Vs (Hall mobility)
Fermi Energy(E_F)	-	80 meV	-	-	43meV	-
Cyclotron mass(m_e)	-	0.13m_e	-	-	0.18m_e	-

Table 4.3: Different parameters of $Bi_2Cu_xTe_{3-x}$ (with x = 0, 0.03, 0.09 and 0.15) at 2K.

composition	**Resistivity**	**Hall parameter**	**AHE amplitude**	**Magnetic moment**
Pure	$1.07X10^{-3}$ Ω-cm	$2.4X10^{-5}$ Ω-cm/T	-	-
x=0.03	$1.36X10^{-4}$ Ω-cm	$8.80X10^{-5}$ Ω-cm/T	-0.10 μΩ-cm	$2.11X10^{-4}$ emu/gm
x=0.09	$6.46X10^{-3}$ Ω-cm	$8.56X10^{-5}$ Ω-cm/T	-0.12 μΩ-cm	$1.35X10^{-3}$ emu/gm
x=0.15	$7.26X10^{-3}$ Ω-cm	$5.74X10^{-6}$ Ω-cm/T	-0.0397 μΩ-cm	$6.13X10^{-3}$emu/gm

We have also determined the bulk carrier mobility of the samples. The calculated mobility (μ) of the carriers are well matched with the reported values in the TIs[84], [113], [115]. However, it is obvious that the mobility calculated from FFT (discussed above) is different

from the Hall mobility indicating that the SdH oscillation is certainly coming from the surface. With doping of Cu (x = 0.09), scattering centers increase resulting lower mobility. The trend remains continued in x = 0.15 sample also, but the presence of significant Cu (x = 0.15) also increases bulk contribution [MR data also support where the absence of SDH oscillations is observed]. As a consequence, very large carrier concentration and low mobility are found in x = 0.15 sample. This might also be the reason of getting the interesting MR behavior with doping content. Interestingly, it is seen that Hall graph was linear for the sample x = 0, but non-linearity is observed with Cu doping. Two type of carrier conduction or anomalous Hall effect (AHE) might be the origin of the nonlinearity. We tried to fit the data with two-carrier model [116], but the obtained parameters were not feasible. Therefore, the observed non-linearity in the Hall curve might be an indication of anomalous Hall effect (AHE). According to Smith et al[18], screw (asymmetric) scattering, which arises from impurities caused by spin–orbit interaction, was the main source of AHE. On the other hand, Berger argued that the main source of AHE was side jump which is experienced by quasi-particles during scattering from spin–orbit coupled impurities. So, the coefficient of anomalous Hall resistivity can be expressed as;

$$R_M = a\rho_{xx0} + b\rho^2 + c\rho^2 \qquad (4.1)$$

where a, b, and c are the constants and ρxx0 is the residual resistivity. First, second and third terms in the expression represents screw scattering, side jump, and intrinsic contribution. In order to get the anomalous Hall contribution, we have subtracted the linear Hall contribution from the Hall data using equation (4.2) as is given below. Presence of AHE has been generally found in materials with magnetic ordering. In a magnetic sample, the Hall

resistivity depends on the applied field as well as magnetization (M) of the materials. Total Hall resistivity can be expressed as:

$$\rho_{xy} = R_0 H + R_{MM} \tag{4.2}$$

The first term in (2) is the normal Hall resistivity whereas the second term is due to the anomalous Hall resistivity coupled to the magnetization. Here R_0 is the Hall coefficient, H is the applied magnetic field, R_M is the anomalous Hall coefficient, and M is the magnetization of the material. At high field, the ordinary Hall effect dominates as is seen by the linear dependence of ρ_{xy} whereas at We have calculated AHE for x = 0.03, 0.09 and x = 0.12 are shown in figures 4.9(a)–(c).

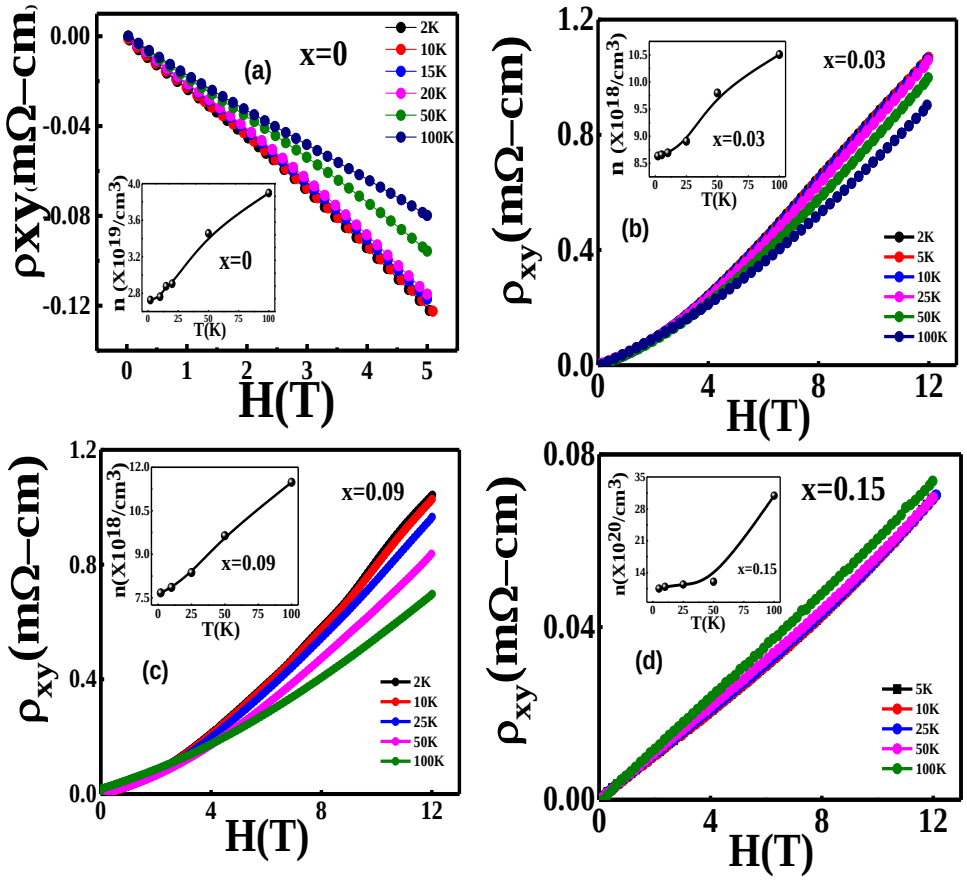

Figure 4.8: The variation of Hall resistivity as a function of applied magnetic fields of $Bi_2Cu_xTe_{3-x}$ for (a) x = 0, (b) x = 0.03 (c) x =0.09 and (d) x = 0.15 at different temperatures.

AHE in x = 0.03 and x = 0.09 have significant value as well as consistent with the temperature. For x = 0.15, the value is very small (almost negligible in comparison to x = 0.03 and 0.09 which is shown in figures 4.9 (c) and 4.9 (d) at different temperatures).

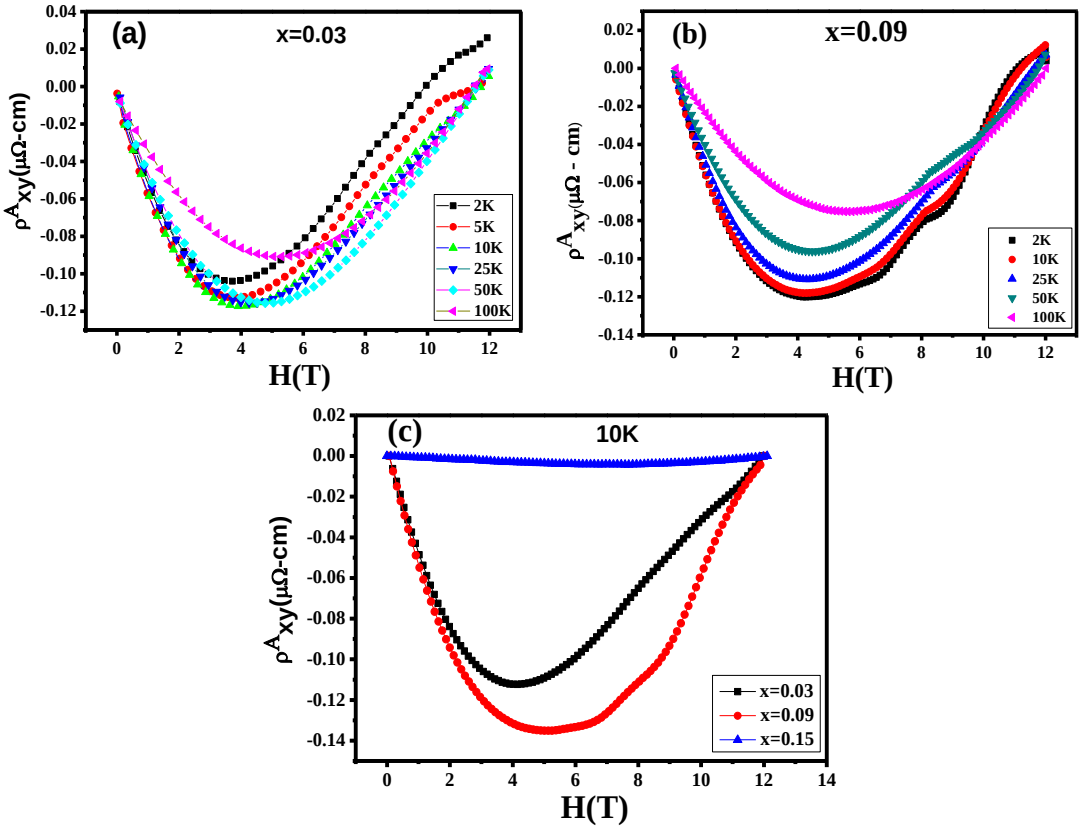

Figure 4.9: Calculated anomalous Hall effect (AHE) of $Bi_2Cu_xTe_{3-x}$ for (a) x = 0.03 and (b) 0.09 at different temperatures. (c) and (d) Estimated AHE at diff. temperatures of $Bi_2Cu_xTe_{3-x}$ for x = 0.03, 0.09, 0.15 at 10 K and 100 K.

In order to confirm the magnetic state present in the samples, magnetization (M) vs. temperature (M–T) and M vs. applied magnetic field (M–H) measurements have been performed [figure 4.10]. It is clear from figure 4.10 (a), that the value of magnetization is positive at low temperature i.e., 4 K and 12 K for the samples x = 0.03 and 0.09 respectively. But, no negative value of magnetization has been found in x = 0.15 sample. For further confirmation of the magnetic ordering in the sample, M–H measurement has been carried out at 2 K. It is clear from the M–H curve that the value of M is increasing as we increase Cu concentration

from x = 0.03 to x = 0.09 but further doping of Cu (x = 0.15) reduces the magnetization value. Diamagnetic background (negative slope) in M–H curve is observed in samples x = 0.03 and x = 0.09 at the higher field around 1.5 T. But no diamagnetic background in M–H curve is observed in x = 0.15 sample even at the highest applied field 2 T which is also consistent with the M–T curve. Moreover, it is noteworthy that the field value, at which M–H curve shows a negative slope, increases with the increasing concentration of Cu. In inset of figure 4.10 (b) at the low applied field existence of hysteresis loop is observed indicating the presence of ferromagnetic state. Increasing value of magnetic moment up to a certain doping concentration and then decrease in magnetization above the doping concentration has also been observed in different diluted magnetic semiconductors (DMS)[117]. To shed more light on the presence of AHE in the doped samples (x =0.03, 0.09 and 0.15), we find that this AHE is not correlated with the ferromagnetism because we get a significant ferromagnetic ordering in x = 0.15 while the value of AHE is negligible in this sample figures 4.9 (c) and 4.9 (d). The x = 0.03 and 0.09 are also showing that the magnetic ordering present in the samples at low temperature and at high temperature they are showing diamagnetic behavior but we get significant AHE up to 100 K in both the samples. Therefore, it is clear that ferromagnetic ordering is not the origin of AHE. In the present system, AHE may be associated with 2D transport inspite of bulk transport [59] and this fact can be successfully described by our SDH-oscillation analysis. We get prominent oscillations and clear signature of surface state in x = 0.03, 0.09 but surface state weakens i.e. x= 0.15 which might be due to the lowering of crystal quality with Cu content. Similarly, we get AHE in x = 0.03, 0.09 with significant value and for x = 0.15 the AHE is negligible in comparison to x = 0.03, 0.09. Hence the

coexistence of AHE and SdH oscillations suggest that the 2D transport in Cu doped Bi_2Te_3 might be the main origin for AHE.

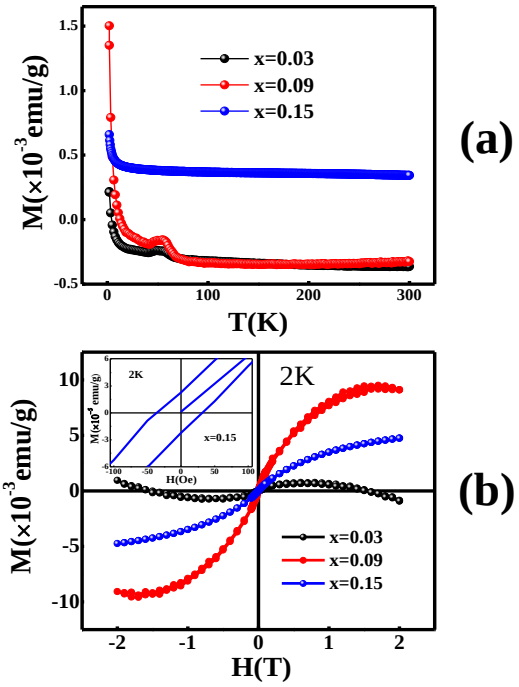

Figure 4.10: (a) Magnetization vs temperature (M –T) and (b) magnetization (M) vs applied magnetic field (M –H) of $Bi_2Cu_xTe_{3-x}$ (with x = 0.03, 0.09 and 0.15).

As has been mentioned the ARPES results also supports the 2D transport. Figure 4.11 (a) and 4.11 (c) shows σ_{xx} vs σ_{AHE} plot on a logarithmic scale. To do this scaling of σ_{AHE}, anomalous hall conductance with σ_{xx}, magneto-conductance, we have used following formulas;

$$\sigma_{xx}=\frac{R_{xx}(B=0)}{\left(R_{sat}^{AHE}\right)^2+(R_{xx})^2(B=0)} \quad \text{and} \quad \sigma_{xy}^{AHE}=\frac{R_{sat}^{AHE}}{\left(R_{sat}^{AHE}\right)^2+(R_{xx})^2(B=0)} \tag{4.3}$$

As we have scaled σ_{xy}^{AHE} vs σ_{xx}^{α} we obtain the value of α as 1.95 for x=0.03 and 2.13 for x=0.09. Moreover, we have calculated AHE angle tan (θ_{AHE}) = $\sigma_{xy}^{AHE}/\sigma xx$ which is shown in figure 4.11 (b) and (d). The value of tan (θ_{AHE}) is increased with decreasing temperature and this behaviour is well matched with other reports [118]. This type of behaviour is consistent with the predicted model [119], [120]. It is well known that in intrinsic AHE, σ_{xy}^{AHE}

remains constant with respect to σ_{xx} as well as side jump mechanism also shows same type of behaviour [120]. It is remarkable that these mechanisms are independent of scattering rate; τ [117], [119] and we cannot separate the intrinsic and side-jump contribution on the basis of τ [117], [119]. According to semiclassical model, both intrinsic and side jump mechanism obeys ρ_{xy} α ρ_{xx}^2[117], [120]. However, in the present case it is more suitable to attribute observed scaling to the intrinsic mechanism because of the existence of the Berry curvature But, the contribution of side jump mechanism also cannot be ruled out. Therefore, it deserves further study to reach out its origin.

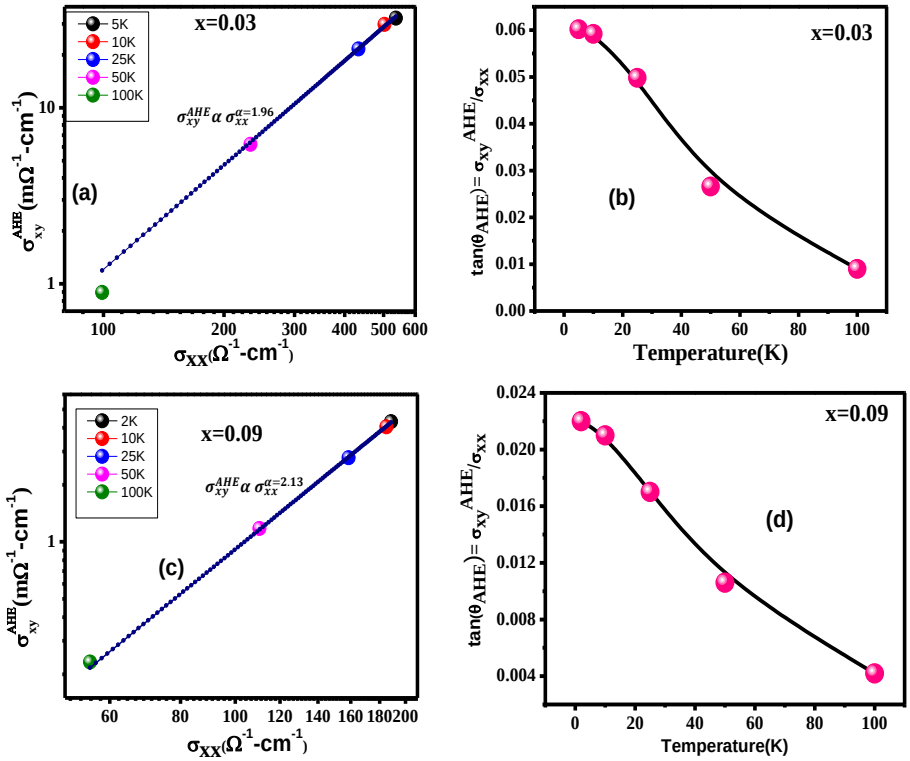

Figure 4.11: (a) and (c) The variation between σ_{xx} and σ_{AHE} and (b), (d) temperature variation of tangent of anomalous Hall angle [tan(θ_{AHE})] for $Bi_2Cu_xTe_{3-x}$ respectively for x = 0.03 and 0.09.

4.4 Conclusion

We have investigated the ARPES and magneto-transport properties of $Bi_2Cu_xTe_{3-x}$ single crystals. ARPES study indicates the clear existence of surface states in the as-prepared

samples. The bandgap for x = 0.03 is 5 meV and that for the x = 0.15 sample the value is 16 meV. Presence of Cu introduces magnetic ordering in Bi_2Te_3 which is clear from magnetic measurement. The occurrence of anomalous Hall effect is not due to the magnetic ordering but due to the 2D transport as is clear from SdH oscillation and from ARPES result.